PROCEEDINGS OF SCIENCE

Timepix3 as a solid-state time-projection chamber in particle and nuclear physics

B. Acharya,[a,2] **J. Alexandre,**[a] **P. Beneš,**[b] **B. Bergmann,**[b] **A. Bevan,**[d] **T. Billoud,**[b] **H. Branzas,**[e] **P. Burian,**[b,f] **M. Campbell,**[g] **S. Cecchini,**[h] **Y. M. Cho,**[i] **M. de Montigny,**[j] **A. De Roeck,**[g] **J. R. Ellis,**[a,k,l] **M. M. H. El Sawy,**[g,m] **M. Fairbairn,**[a] **D. Felea,**[e] **M. Frank,**[n] **D. Garvey,**[b] **J. Hays,**[d] **A. M. Hirt,**[o] **J. Janeček,**[b] **M. Kalliokoski,**[p] **A. Korzenev,**[q] **D. H. Lacarrère,**[g] **C. Leroy,**[r] **G. Levi,**[s] **A. Lionti,**[q] **P. Mánek,**[b,3] **A. Maulik,**[h,j] **A. Margiotta,**[s] **N. Mauri,**[h] **N. E. Mavromatos,**[a] **L. Meduna,**[b] **P. Mermod,**[q] **L. Millward,**[d] **V. A. Mitsou,**[c] **I. Ostrovskiy,**[t] **P.-P. Ouimet,**[j,u] **J. Papavassiliou,**[c] **B. Parker,**[v] **L. Patrizii,**[h] **G. E. Păvălaş,**[e] **J. L. Pinfold,**[j] **L. A. Popa,**[e] **V. Popa,**[e] **M. Pozzato,**[h] **S. Pospíšil,**[b] **A. Rajantie,**[w] **R. Ruiz de Austri,**[c] **Z. Sahnoun,**[h,x] **M. Sakellariadou,**[a] **A. Santra,**[c] **S. Sarkar,**[a] **G. Semenoff,**[y] **A. Shaa,**[j] **G. Sirri,**[h] **K. Sliwa,**[z] **P. Smolyanskiy,**[b] **R. Soluk,**[j] **M. Spurio,**[s] **M. Staelens,**[j] **M. Suk,**[b] **M. Tenti,**[1] **V. Togo,**[h] **J. A. Tuszyński,**[j] **A. Upreti,**[t] **V. Vento,**[c] **O. Vives,**[c] **A. Wall**[t] **and E. White**[b]

[a] *Theoretical Particle Physics & Cosmology Group, Physics Dept., King's College London, UK*
[b] *IEAP, Czech Technical University in Prague, Czech Republic*
[c] *IFIC, Universitat de València - CSIC, Valencia, Spain*
[d] *School of Physics and Astronomy, Queen Mary University of London, UK*
[e] *Institute of Space Science, Bucharest - Măgurele, Romania*
[f] *Faculty of Electrical Engineering, University of West Bohemia, Pilsen, Czech Republic*
[g] *Experimental Physics Department, CERN, Geneva, Switzerland*
[h] *INFN, Section of Bologna, Bologna, Italy*
[i] *Center for Quantum Spacetime, Sogang University, Seoul, Korea*
[j] *Physics Department, University of Alberta, Edmonton, Alberta, Canada*
[k] *National Institute of Chemical Physics & Biophysics, Tallinn, Estonia*
[l] *Theoretical Physics Department, CERN, Geneva, Switzerland*
[m] *Basic Science Department, Faculty of Engineering, The British University in Egypt, Cairo, Egypt*
[n] *Department of Physics, Concordia University, Montréal, Québec, Canada*
[o] *Department of Earth Sciences, Swiss Federal Institute of Technology, Zurich, Switzerland*
[p] *Helsinki Institute of Physics, University of Helsinki, Finland*
[q] *Département de Physique Nucléaire et Corpusculaire, Université de Genève, Geneva, Switzerland*
[r] *Département de Physique, Université de Montréal, Québec, Canada*
[s] *INFN, Section of Bologna & Department of Physics & Astronomy, University of Bologna, Italy*
[t] *Department of Physics and Astronomy, University of Alabama, Tuscaloosa, Alabama, USA*
[u] *Physics Department, University of Regina, Regina, Saskatchewan, Canada*
[v] *Institute for Research in Schools, Canterbury, UK*

PoS(ICHEP2020)720

[w] *Department of Physics, Imperial College London, UK*
[x] *Centre for Astronomy, Astrophysics and Geophysics, Algiers, Algeria*
[y] *Department of Physics, University of British Columbia, Vancouver, British Columbia, Canada*
[z] *Department of Physics and Astronomy, Tufts University, Medford, Massachusetts, USA*
[1] *INFN, CNAF, Bologna, Italy*
[2] *Int. Centre for Theoretical Physics, Trieste, Italy*
[3] *Department of Physics and Astronomy, University College London, London, UK.*
E-mail: benedikt.bergmann@utef.cvut.cz

Timepix3 devices are hybrid pixel detectors developed within the Medipix3 collaboration at CERN providing a simultaneous measurement of energy (ToT) and time of arrival (ToA) in each of its 256×256 pixels (pixel pitch: 55 µm). The timestamp resolution below 2 ns allows a measurement of charge carrier drift times, so that particle trajectories can be reconstructed in 3D on a microscopic level (z-resolution: 30-60 µm). The 3D trajectory reconstruction methodology developed elsewhere is validated against simulated data providing ground truth information of the incident angles. The detector response functions and the achievable track angular resolutions are determined. For the first time, data taken with Timepix3 in the MoEDAL experiment are presented. After extracting singly charged minimum ionizing particle (MIP) tracks from the mixed radiation field using characteristic track features, their impact angles are evaluated. The directionality of the MIP radiation field is shown in elevation angle (θ) versus azimuthal angle (ϕ) maps, "unfolded" using the simulated detector responses to an omnidirectional radiation field.

40th International Conference on High Energy physics - ICHEP2020
July 28 - August 6, 2020
Prague, Czech Republic (virtual meeting)

1. Introduction

High-energy physics (HEP), nuclear physics, space research and medical physics depend on fast and reliable detector systems to measure radiation levels, identify particles and determine their direction and energy. Hybrid pixel detectors (HPDs) enable noiseless detection and processing of individual particle events. It was shown that HPDs of Timepix3 technology can be regarded as solid-state Time-Projection-Chambers (TPCs) allowing 3D particle trajectory reconstruction together with the measurement of the energy left in the sensor material [1, 2]. Compared to gas-filled TPCs, semiconductor TPCs offer an increased speed of operation and a ~10 × lower energy needed to create free charge carriers.

An application of Timepix3 in HEP can be found in the ATLAS experiment, where it has proven valuable for the measurement of luminosity and the composition of the radiation field. With a time resolution below 2 ns, the bunch structure of the LHC beam can be resolved and particle tracks can be assigned to their corresponding bunches [3]. Another LHC experiment using Timepix3 detectors is MoEDAL (Monopole and Exotics Detector At the LHC) [4], dedicated to the search for magnetic monopoles and massive highly ionizing (pseudo-) stable particles [5]. While MoEDAL primarily relies on passive nuclear track detectors (NTDs) and paramagnetic trapping volumes, Timepix and Timepix3 detectors are installed at different locations to provide a real-time measurement of the radiation levels and means to decompose the radiation field. In the present work, the track reconstruction methodology from [1, 2] is firstly applied to simulated data to model the angular detector response for Minimum Ionising Particles (MIPs). After MIPs are extracted from the mixed field data taken in MoEDAL the methodology is used to measure their directionality.

2. Detector technology and methodology

Timepix3: Timepix3 is fabricated in the 130 nm CMOS technology and divides the sensor into a square matrix of 256×256 pixels with a pixel pitch of 55 μm. Timepix3 features a data-driven readout scheme allowing for measurements with negligible dead-time up to pixel hit rates of 40 MHits s^{-1} cm^{-2}. In data-driven mode, only the pixel triggered by the interaction of an ionizing particle in the sensor is read out, while all other pixels in the matrix stay active. The per-pixel dead time is ~475 ns. In each pixel, the energy deposition (ToT) and the time of the interaction (ToA) are determined simultaneously. The ToA is measured with a precision of 1.56 ns. The necessary energy calibration and time-walk correction methodology is described in [6] and [1, 2], respectively.

3D trajectory reconstruction: Ionizing particles interacting in the fully depleted sensor create free charge carriers (electrons e^- and holes h^+) which start to drift due to an applied electric field between the (common) back side and the pixel contacts. During their drift motion, these charge carriers induce currents at the pixel electrodes [7] which are processed (shaped, amplified and digitized) to determine ToA and ToT. Due to the high ratio of sensor thickness and pixel pitch, a detectable signal is only created if the charge carriers are in close vicinity to the pixel electrodes (small-pixel effect). Thus, charge carriers initially created farther away from the pixel contacts generate a delayed signal when compared with concurrent ones created at closer distance. Another consequence of the small pixel effect is that the majority of the signal induced on a collecting electrode is due to either e^- or h^+ movement, depending on the sensor used and polarity of the bias

voltage. Using the known relation of the drift velocity as a function of the electric field, the drift time dependence on interaction depth can be determined analytically for silicon [2] or numerically for CdTe sensors [1]. It was found that a z-resolution of ~30 μm and ~60 μm can be achieved in 500 μm thick silicon and 2 mm thick CdTe sensors, respectively. For the 500 μm thick (p^+-in-n) silicon sensor used in the present work, the dependency of the interaction depth z on drift time t_{drift} is given by:

$$z(t) = \frac{d}{2\,U_{\text{D}}}(U_{\text{D}} + U_{\text{B}})\left[1 - \exp\left(-\frac{2\,U_{\text{D}}\,\mu_{\text{h}}}{d^2}t_{\text{drift}}\right)\right], \tag{1}$$

with the sensor thickness $d = 500\,\mu$m, the depletion voltage $U_{\text{D}} = 100$ V, the hole mobility $\mu_{\text{h}} = 450\,\frac{\text{cm}^2}{\text{V s}}$ and the bias voltage U_{B} which was set at 230 V.

3. Data analysis

Figure 1 shows a snapshot of the radiation field measured with Timepix3 during Pb-ion runs in the MoEDAL experiment. Clusters, i.e. traces left by ionizing particles, with a different number of pixels, energy deposition and curvature are seen. As discussed e.g. in [3, 8, 9] such morphological features can be used for a basic classification of tracks in the radiation field.

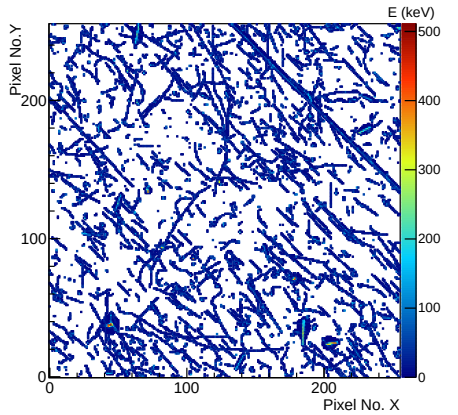

Figure 1: Frame showing tracks accumulated during 1 s in MoEDAL (Fill 7472 on November 25, 2018).

Track selection: In the radiation field shown in Fig. 1, the majority of tracks appears to be oriented. To assess the directionality, traces of particles with low stopping power (MIPs) fully penetrating the sensor were selected by the following conditions:

- The drift time difference within the track should exceed 20 ns;
- The maximum energy in a single pixel of the track is below 180 keV;
- The linearity of the track, defined as the number of pixels lying on a line between the two endpoints divided by the total number of pixels in the track, is above 80 %;
- The number of pixels in the track is greater than 4, whereby the track length projected to the xy-plane is greater than 2.

Simulation: Simulations were performed with an in-house developed Geant4 [10] simulation tool to understand the angular response and the effect to the above defined track selection cuts. The energy depositions E_{dep} along the particle track are sampled in steps of 5 μm. At each location in the sensor $\vec{r}_i$ (i is the step number), the amount of charge carriers was calculated as $N = \frac{E_{\text{dep}}}{3.6\,\text{eV}}$[1]. Diffusion and repulsion of charge carriers during the drift was taken into account. The ToA was determined by the holes with the lowest drift times. The energy was given by the total amount of charge registered in the pixel. An energy-dependent Gaussian ToA noise, gradually decreasing from $\sigma_{\text{ToA}} = 4$ ns at 3.9 keV to $\sigma_{\text{ToA}} = 1.2$ ns at 25 keV, and a Gaussian ToT noise with a width of 200 e^-

[1] 3.6 eV is the energy needed to create an electron-hole pair in silicon [11].

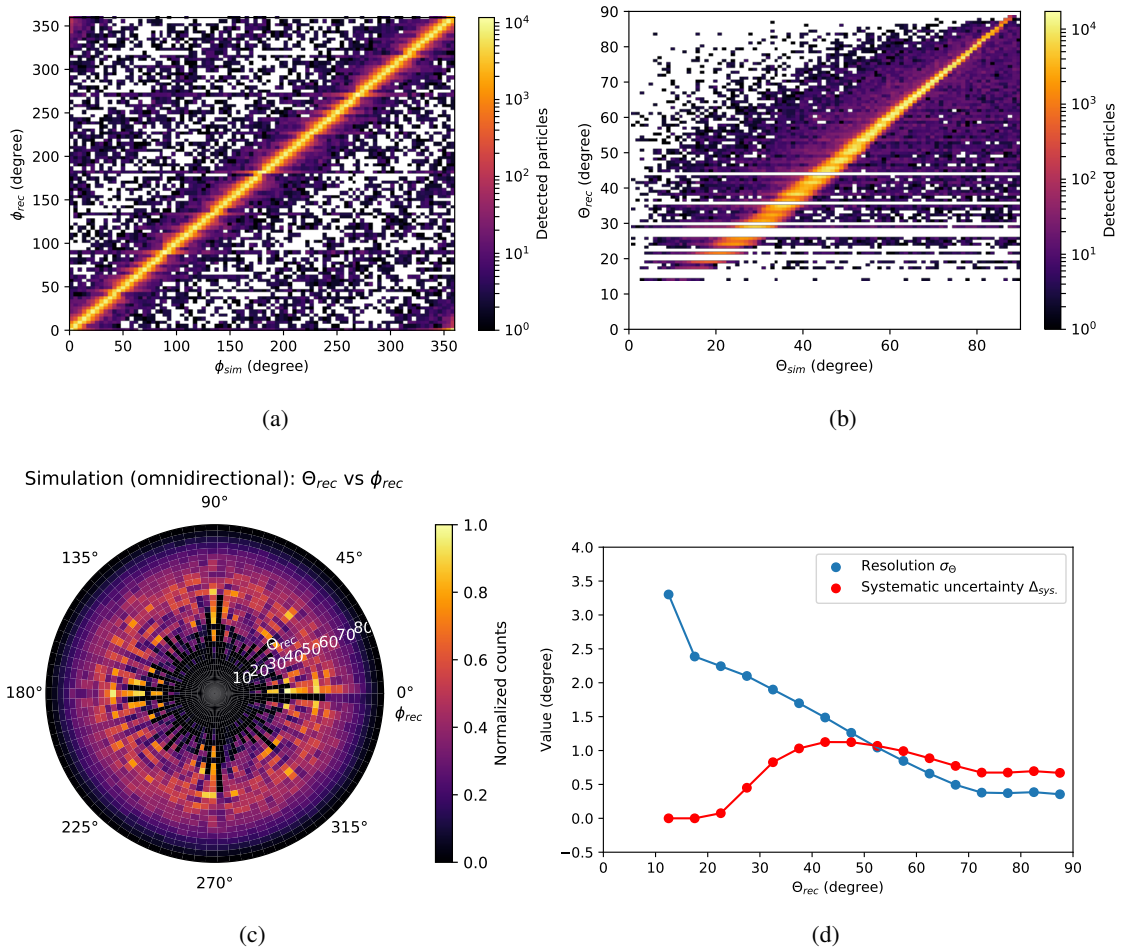

Figure 2: Scatter plots of the "reconstructed" angles versus (a) the simulated azimuthal angle ϕ_{sim} and (b) the simulated elevation angle θ_{sim}; (c) Detector response matrix (θ_{rec} vs ϕ_{rec}) to an omnidirectional radiation field: $R^{\text{omni}}_{i,j}$; (d) Systematic error Δ_{sys} and resolution σ_θ as a function of the elevation angle θ_{rec} (see text).

(720 eV) were added in each pixel. Pixels with energies below a threshold of 2.7 keV were omitted. Pions of 40 GeV energy were emitted isotropically from a spherical source of radius 2.5 cm around the detector. For each registered event the "true" impact angle and the angle reconstructed from the pixel data are stored.

Angular response: Figures 2(a) and 2(b) show the angular response matrices. The azimuthal angle ϕ is defined as the angle with respect to the x-axis of the pixel matrix, the elevation angle θ is the angle with respect to the sensor normal. For both angles an excellent linear response is found. To study the achievable resolution and the systematic errors of the θ determination, the distributions of the differences $\Delta\theta = \theta_{\text{sim}} - \theta_{\text{rec}}$ were created for 16 θ intervals and fitted with a Gaussian distribution. The widths of these distributions are interpreted as the resolution σ_θ, their mean values are interpreted as a systematic error Δ_{sys}. σ_θ and Δ_{sys} are shown as a function of the reconstructed elevation angle in Fig. 2(d).

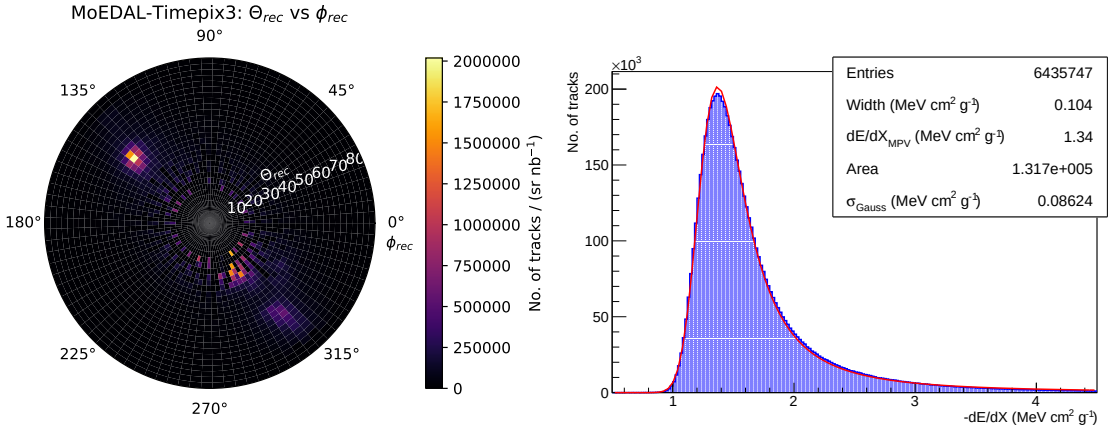

(a) (b)

Figure 3: MoEDAL experiment - Fill 7472: (a) Corrected directionality map; (b) Energy loss spectrum of particles passing through the sensor fitted with a Landau-Vavilov with Gaussian smearing.

4. Results

Data taken by Timepix3 in the MoEDAL experiment [4] during Pb-ion runs in Fill 7472 on November 25, 2018 with a run-integrated luminosity of 0.013 nb^{-1} were evaluated. Figure 3(a) shows the directionality of the radiation field in a θ-vs-ϕ map $M^{\mathrm{corr.}}_{i,j}$. The raw measured map $M_{i,j}$ was hereby corrected for cut and solid angle acceptances using bin-by-bin division with the normalized detector response to an omnidirectional radiation field $R^{\mathrm{omni}}_{i,j}$ shown in Fig. 2(c): $M^{\mathrm{corr.}}_{i,j} = \frac{M_{i,j}}{R^{\mathrm{omni}}_{i,j}}$, where i and j label the bins in ϕ and θ, respectively. The results indicate a highly directional radiation field with the primary peak (at $\theta \approx 45°$, $\phi \approx 135°$) pointing towards the interaction point. Secondary peaks shifted by 180° to the primary peak are assumed to be due to particles interacting in the beam pipe or in collimators. Figure 3(b) shows the energy loss per unit length of tracks used for the directionality map. It is consistent with a Landau-Vavilov distribution convolved with a Gaussian. A most probable value $dE/dX_{\mathrm{MPV}} = (1.3391 \pm 0.0001)\,\mathrm{MeV\,cm^2\,g^{-1}}$ was found, which is consistent with the value for minimum ionizing particles with a nuclear charge $Z = 1$ in silicon.

5. Discussion

In the present work, the 3D track reconstruction capability of a Timepix3 detector was studied in a simulation and applied to data taken in the MoEDAL experiment. MIPs were selected from a mixed radiation field. Their directionality was shown in a θ-vs-ϕ map. Hereby, MIP selection cut and angular acceptances were corrected for using the simulated detector response.

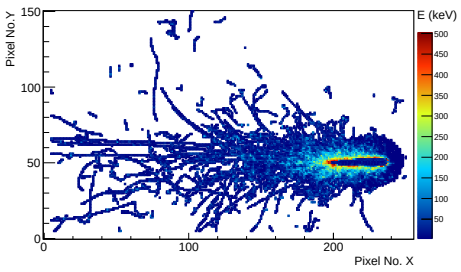

Figure 4: 330 GeV/c Pb ion at $\theta = 75°$ measured at the Super-Proton-Synchrotron.

Besides the tracking performance, Timepix3 allows a separation of different particle species using the dE/dX information together with other char-

acteristic track features, such as the number, angular distribution and the energy deposition of δ-electrons. Measurements of the detector response in radiation fields of known composition have been started. The experimentally determined database covers a broad range of particles and energies: from protons of few hundreds of MeV to heavy ions in the GeV range, see Fig. 4. Current efforts focus on the development of models to separate different particles using machine learning approaches.

Acknowledgments

The work was done within the Medipix3 collaboration. The work has further profited from the European Regional Development Fund-Project "Engineering applications of physics of microworld" (No. CZ.02.1.01/0.0/0.0/16_019/0000766) and the STFC (UK) grant ST/T000759/1 It was supported by the Generalitat Valenciana via a special grant for MoEDAL and the projects PROMETEO-II/2017/033 and PROMETEO/2019/087 from MCIU / AEI / FEDER, EU via the grants FPA2016-77177-C2-1-P, FPA2017-85985-P, FPA2017-84543-P and PGC2018-094856-B-I00. The support of NSERC-Canada is gratefully acknowledged.

References

[1] B. Bergmann et al. 3D reconstruction of particle tracks in a 2 mm thick CdTe hybrid pixel detector. *Eur. Phys. J. C*, 79(165), 2019.

[2] B. Bergmann et al. 3D track reconstruction capability of a silicon hybrid active pixel detector. *Eur. Phys. J. C*, 77(421), 2017.

[3] B. Bergmann et al. Particle tracking and radiation field characterization with Timepix3 in ATLAS. *Nucl. Inst. Meth. A*, 978:164401, 2020. ISSN 0168-9002.

[4] J. Pinfold. The MoEDAL experiment at the LHC. *EPJ Web Conf.*, 145:12002, 2017.

[5] B. Acharya and others MoEDAL collaboration. The physics programme of the moedal experiment at the lhc. *Int. J. Mod. Phys. A*, 29(23):1430050, 2014.

[6] P. Burian et al. Katherine: Ethernet Embedded Readout Interface for Timepix3. *JINST*, 12 (11):C11001, 2017.

[7] S. Ramo. Currents induced by Electron Motion. In *Proceedings of the I.R.E*, volume 27, pages 584–585, Sept. 1939. doi: 10.1109/JRPROC.1939.228757.

[8] N. Asbah et al. Measurement of the efficiency of the pattern recognition of tracks generated by ionizing radiation in a TIMEPIX detector. *JINST*, 9(05):C05021–C05021, May 2014.

[9] B. Bergmann et al. Characterization of the Radiation Field in the ATLAS Experiment With Timepix Detectors. *IEEE Transactions on Nuclear Science*, 66(7):1861–1869, 2019.

[10] S. Agostinelli et al. Geant4—a simulation toolkit. *Nucl. Inst. Meth. A*, 506(3):250 – 303, 2003. ISSN 0168-9002.

[11] A. Owens. *Compound Semiconductor Radiation Detectors*. CRC Press, Taylor & Francis Group, 6000 Broken Sound Parkway NW, Suite 300, 2012. ISBN 978-1-4398-7312-0.